AIAA JOURNAL
Vol. 41, No. 12, December 2003

Dynamics and Control of an Isolated Jet in Crossflow

S. Narayanan*
United Technologies Research Center, East Hartford, Connecticut 06108
P. Barooah†
University of California, Santa Barbara, Santa Barbara, California 93111
and
J. M. Cohen‡
Pratt and Whitney, East Hartford, Connecticut 06108

Experimental results from a systematic exploration of the dynamics and control of large-scale, organized structures in an isolated, circular jet issuing into a uniform crossflow with a jet-to-crossflow velocity (or blowing) ratio of 6 are presented. Surveys of the unsteady flowfield were conducted using a single sensor hot-film probe, and the instantaneous and time-averaged scalar fields were explored using Mie scattering-based flow visualization. A spinning mechanical valve was used to modulate the jet flow with a single frequency. The forced flow response illustrates the flow receptivity to high frequencies near the jet exit (associated with the jet instabilities) and to low frequencies farther downstream (where the counter-rotating vortex pair dynamics are dominant). Open-loop forcing in a jet Strouhal number around $Sr_D = 0.1$ was recognized and demonstrated to be effective in organizing unsteadiness and enhancing mixing and entrainment in the flowfield. Measurements of the time-averaged velocity and scalar fields are used to demonstrate increased mass entrainment and mixing as a result of the unsteady forcing.

Nomenclature

A	=	cross-sectional area of channel, m^2
D_j	=	diameter of jet nozzle, m
f	=	frequency, Hz
h	=	channel height, m
l	=	flow structure length scale, m
Re	=	Reynolds number, $(U D_j/\nu)$
r	=	velocity ratio, (U_j/U_∞)
Sr_D	=	Strouhal number, identical to $f D_j/U$
U	=	local mean velocity, m/s
U_j	=	jet exit velocity, m/s
U_∞	=	crossflow velocity, m/s
u'	=	local turbulence intensity, m/s
x	=	axial distance, 0 at jet centerline
y	=	vertical distance, 0 at jet injection wall
z	=	spanwise distance in channel, 0 at center
δ	=	boundary-layer thickness on channel horizontal wall, m
ν	=	kinematic viscosity for air, m^2/s
ρ	=	density of air at room temperature, kg/m^3

I. Introduction

JETS in crossflow are used in several applications such as thrust vectoring[1] and dilution jets for combustion.[2] It has been known that the forcing of jets exiting into quiescent fluid can have a substantial impact on the structure and mixing of the jet. The optimal forcing frequencies for increased jet mixing are claimed[3] to correspond to a nondimensional forcing frequency of $Sr_D(\equiv f D_j/U_j) = 0.4$, based on the forcing frequency f, jet diameter D_j, and jet velocity U_j. Enhanced entrainment and mixing are caused by large-scale vortical structures excited in the jet shear layer. Consequently, similar forcing of the shear layer of a jet in crossflow has been attempted, although forcing at lower excitation frequencies was shown to be effective.[4–6] However, the beneficial nondimensional forcing frequency range reported varies significantly in the range $0.004 < Sr_D < 0.22$. Several forcing parameters have been considered, in addition to the forcing frequency, over a range of jet-to-cross-stream velocity ratios, such as the forcing amplitude, duty cycle (i.e., the fraction of the forcing period over which a pulse is injected), and the shape of the forcing signal waveform. Although the forcing waveforms input to the actuators are different, the velocity fluctuations imposed on the flow were seldom measured, and they may have varied significantly. In general, forced transverse jet data identifying the dominant underlying flow structure dynamics appears to be scarce. Only recently have attempts to characterize the actuation system for the forced jet in crossflow been reported and used systematically to develop jet control schemes.[7]

In the present study, we aim to understand the intrinsic dynamics of the jet in crossflow via forced response tests and then utilize this for open-loop control to enhance the mixing of an isolated jet in crossflow. This approach is in contrast to prior studies that attempted to maximize mixing and/or penetration of jets in crossflow by testing a variety of forcing techniques and waveforms and then analyzing the excited flowfields to explain the underlying mechanisms. For instance, M'Closkey et al.[7] found that optimal jet penetration and spread was achievable for square wave excitation at subharmonics of the natural vortex shedding frequency of the jet with specific duty cycles.

The jet in crossflow, consisting of a jet emerging perpendicularly from an orifice into a uniform channel flow, has a complex, three-dimensional flow structure. Kelso et al.[8] provide a detailed review of the dominant flow structures. The shear layer along the upstream edge of the jet develops oscillations that roll up into vortical blobs and advect along the jet axis. As the jet bends into the cross stream, a counter-rotating vortex pair (CVP) forms and entrains crossflow fluid. The details of the mechanism underlying the formation of the CVP is a subject of ongoing research. Most studies attribute the CVP formation to be intimately connected with the folding and tilting of the ring-type initial jet shear layer vortices,[8–10] particularly for velocity ratios $(r \equiv U_j/U_\infty)$ in the range 5–10. In this velocity ratio range and for high-Reynolds-number flows,[8] that is, $Re \equiv U_\infty D_j/\nu > 400$, wake vortices shedding unsteadily behind the primary jet were seen. Horseshoe or necklace vortices were seen for low-Reynolds-number $Re < 1500$ flows,[11,12] wherein the oncoming channel flow boundary-layer thickness is larger than the

Received 13 November 2002; revision received 11 June 2003; accepted for publication 12 June 2003.

*Project Leader, PW Program Office. Member AIAA.
†Graduate Student, Department of Electrical and Computer Engineering.
‡Manager, Aerodynamics, CAN Advanced Technology Group. Associate Fellow AIAA.

jet diameter. We focus our attention on the jet shear layer dynamics, which can be controlled via manipulation of the jet initial conditions, and the dynamics of the CVP, which are largely responsible for the cross-stream mixing. These flow structures seem to be the dominant ones for the velocity ratio $r = 6$ considered here.

Our objective is to evaluate the effect of periodic forcing on mixing by a jet in crossflow and to determine the most excitable and most beneficial forcing frequencies. Prior studies have focused on identifying and understanding the most beneficial forcing frequencies, namely, those that enhance metrics such as mixing and jet penetration. In addition to exploring this in the present study, we investigate the most excitable dynamics, associated with frequencies that are preferentially amplified in the flowfield such as those arising from instabilities and coherent structures. It is not clear how the range of beneficial and excitable frequencies are related, and this has not been addressed or exploited for control.

We present detailed measurements of the time-averaged and unsteady features of an isolated jet in crossflow focusing on the dynamics and mixing in a near-field flow region involving the unsteady evolution of the jet shear layer structures and their coupling to the formation and dynamics of the three-dimensional CVP structure. The majority of measurements discussed in this paper are restricted to the first six jet diameters D_j from the jet exit (shown subsequently), which for a velocity ratio $r = 6$ flow translates to a length scale $rD_j = 1$; note that the global length scale rD_j allows scaling and comparisons between transverse jets with various velocity ratios. Pratte and Baines[13] claim that the far field of a jet in crossflow begins after $rD_j = 3$, where the CVP structure is considered to be fully developed. Therefore, it should be noted that a bulk of the present measurements and interpretations are valid only in the near field of the flow, where the CVP formation can be manipulated for enhancing mixing. A companion direct numerical simulation-based study of a forced jet in crossflow was also performed to evaluate various mixing metrics and the impact of sinusoidal forcing on them.[2]

II. Experimental Facility

The subscale experiments were performed in the cold, nonreacting environment of a 3-mm-diam incompressible circular jet issuing into a test section of a 11.75×11.75 cm channel with uniform crossflow. The facility is schematically shown in Fig. 1. A large settling chamber precedes the test section with two pairs of perforated plates, which sandwich an air filter followed by a 7.6-cm-long honeycomb. These flow conditioners are followed by a finer mesh screen, which leads to a contoured 10:1 area ratio contraction through which low-turbulence level, uniform airflow is delivered to the 37.5-cm-long test section; finally, the air exits into the laboratory ambient. The streamwise pressure gradient introduced in the test section (with a length-to-height ratio of 3.2) is believed to be negligible, even when the small jet flow is introduced (roughly halfway between the contraction exit and the test section opening to the ambient). The air jet velocity was chosen to be 24.4 m/s, and the channel freestream airflow speed was chosen to be 4.07 m/s to provide a velocity (or blowing) ratio of 6. This choice of the airspeeds enabled a moderate jet Reynolds number (based on jet diameter and jet velocity) of 5×10^3 in which reliable, unsteady, high-response velocity measurements could be made. The Reynolds number based on channel height and cross-stream flow speed was 2.75×10^4. The oncoming channel boundary layer was verified to be turbulent with a uniform core flow having freestream turbulence intensity levels around 2%. The channel boundary-layer thickness δ was verified to be thin compared to the jet diameter, having $\delta/D_j < 0.3$.

Single hot-film anemometry was used to survey the mean and unsteady velocity characteristics of the flowfield; the TSI 1210-20 hot-film sensor used had a frequency response of up to 100 kHz with reliable turbulence spectra measurements up to 10 kHz (without requiring additional corrections). When the accuracy of the hot-film measurements and the repeatability of flow condition setting are considered, a $\pm 2\%$ uncertainty in the mean velocity measurements and a $\pm 5\%$ uncertainty in measurements of the fluctuating component of the velocity exists. The single-sensor hot-film probe was introduced in an end on configuration into the test section from the downstream opening of the test section (Fig. 1), where the cross-stream flow dumped into the ambient. Thus, the resultant of longitudinal and transverse velocity components was measured. Because of a significant crossflow, reverse flow regions do not exist near the jet or in the mixing region of the jet as it bends into the cross stream. Depending on whether velocity measurements were made in the vertical portion of the jet or in the bent (horizontal) portion of the jet in crossflow, the orientation of the hot-film probe relative to the dominant flow vector was different, namely, parallel to the probe support axis in the former case and perpendicular to it in the latter. Accordingly, two different calibrations were conducted and applied to the two different measurement modes in the respective flow regions.

Instantaneous and time-averaged Mie scattering-based imaging were used to visualize the flowfields in a streamwise and several cross-stream planes. Details of this technique are described by Vranos and Liscinsky.[14] A commercially available (Elven) smoke generator was used to provide (submicrometer sized) vaporized mineral oil seed into the jet stream. A 2-W argon ion laser was used to provide a 0.5-mm thin laser sheet for the imaging. The time-averaged scalar images, displayed as a mixture fraction (computed as the ratio of the scattered scalar intensity to the maximum intensity in an image), were acquired by an electronically cooled Photometrics charge-coupled device camera using a 10-s exposure and provided a spatial resolution of 7 pixels/mm. The uncertainty in measurements of the mixture fraction is on the order of $\pm 10\%$ (Ref. 14). Instantaneous scalar images were acquired using a NAC high-speed camera at 200 frames/s providing a 5-ms exposure.

A mechanical spinning valve[15] was used to modulate the jet flow with a single frequency, providing excitation in the frequency

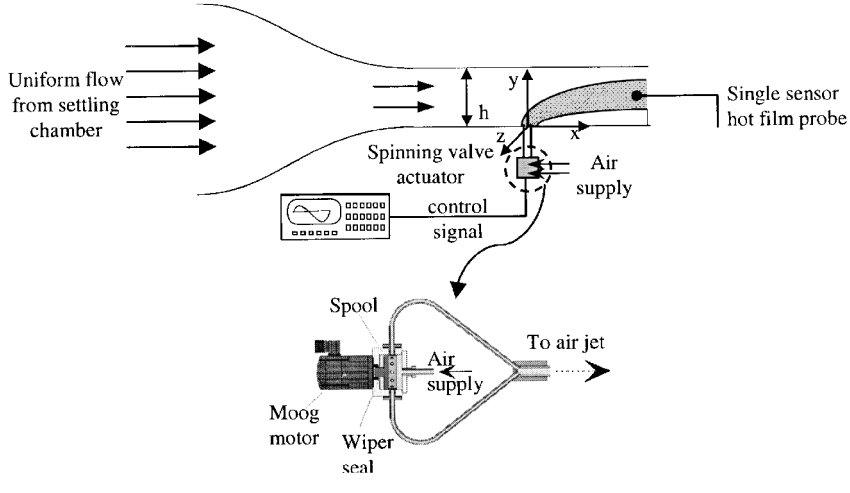

Fig. 1 Schematic of experimental facility and setup of mechanical spinning valve for unsteady jet forcing.

range of 100–1600 Hz corresponding to $0.012 < Sr_D < 0.2$. The nondimensional frequency Strouhal number Sr_D is based on the jet diameter D_j and peak jet velocity for all cases presented henceforth. Figure 1 schematically shows the experimental setup, showing the excitation technique and the spinning valve actuator. The valve-based actuator is described in detail by Barooah et al.,[15] and we supply a brief description in the following. Air supply was provided to a plenum inside a rotating drum (which was connected to a dc motor spool) with 12 small circular holes around the periphery. Concentric to the rotating drum was an outer stationary cylinder, which had two diametrically opposed circular holes connected to a pair of 3-mm-diam tubes. When the motor was operated at a fixed speed, air was delivered to the two outer (stationary) drum holes in a periodic fashion. (The frequency is determined by the number of holes on the rotating drum and the rotor speed.) Thus, a periodic (in-phase) jet flow issued from the two tubes. When the motor used to actuate the valve was not operated, nearly steady flow issued from the two exit ports. The jet is believed to be only partially modulated because of a dc bias flow resulting from leakage within the valve. This was seen in the measured actuator response (shown subsequently and discussed in Sec. III.B), having nonzero airflow from the spinning valve at all times. Long tubes (nearly 50 mm) with large radius bends to minimize flow distortion were used to transport the flow from the outer cylinder to the test section with the crossflow (inset in Fig. 1). The two tubes merged into a straight, 12-mm-long, 3-mm-diam tube, which delivered the air jet into the test section. Normalized profiles of the unforced jet mean velocity and turbulence intensity measured using a single-sensor hot-film probe at the jet exit are shown in Fig. 2. The straight tube was kept short (with a pipe length-to-diameter ratio of nearly 4) to improve actuator authority and frequency response; yet this seems to be sufficient to provide a fully developed mean velocity profile at the exit.

III. Experimental Results

The dynamics in the flow were explored using velocity spectra from the hot-film probe positioned at various locations within and outside the jet as it emerged and bent into the crossflow. These were first conducted in the unforced flow to reveal the underlying natural dynamics and then in forced flows. These were followed by proof-of-concept, open-loop control experiments to demonstrate the mixing and entrainment benefits.

A. Unforced Flowfield and Dynamics

Figure 3 shows instantaneous streamwise (x, y) and cross-stream (y, z) Mie scattering image snapshots of a jet in crossflow. Also

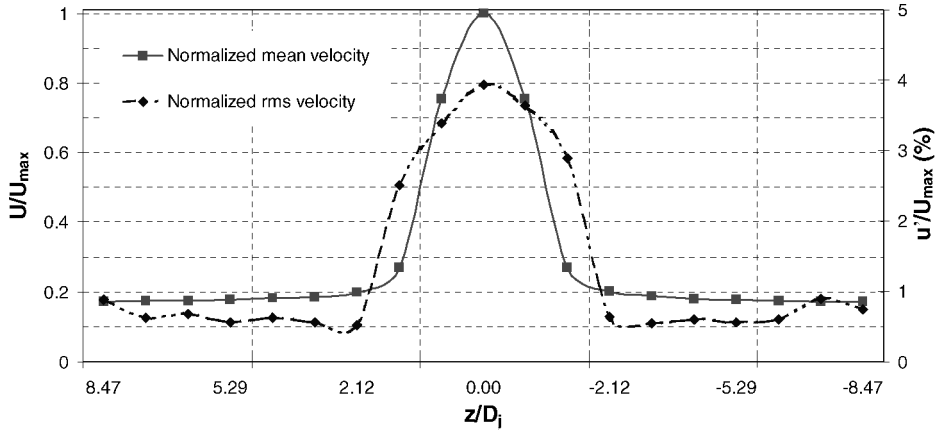

Fig. 2 Profile of mean and fluctuating component of longitudinal velocity at jet exit plane.

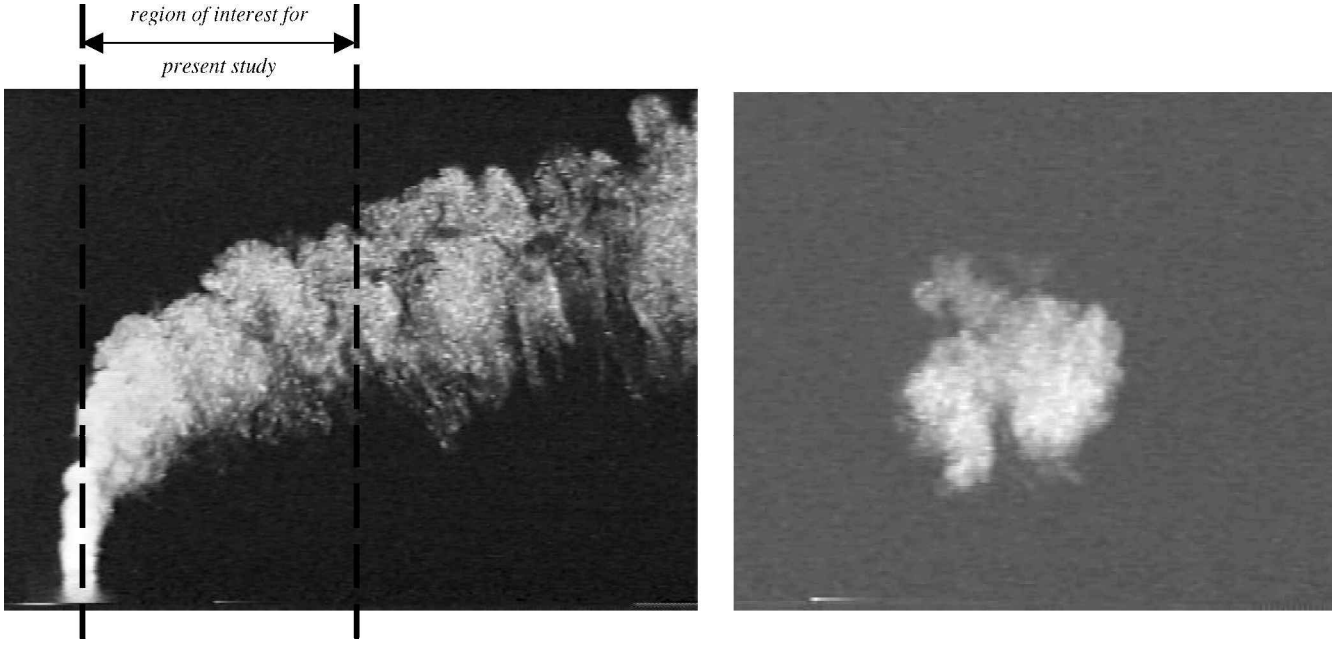

a) **b)**

Fig. 3 Instantaneous scalar images of the unforced jet in crossflow: a) streamwise plane (through the spanwise jet centerline) and b) cross-stream plane (at $x/D_j = 3$ downstream of the jet exit plane).

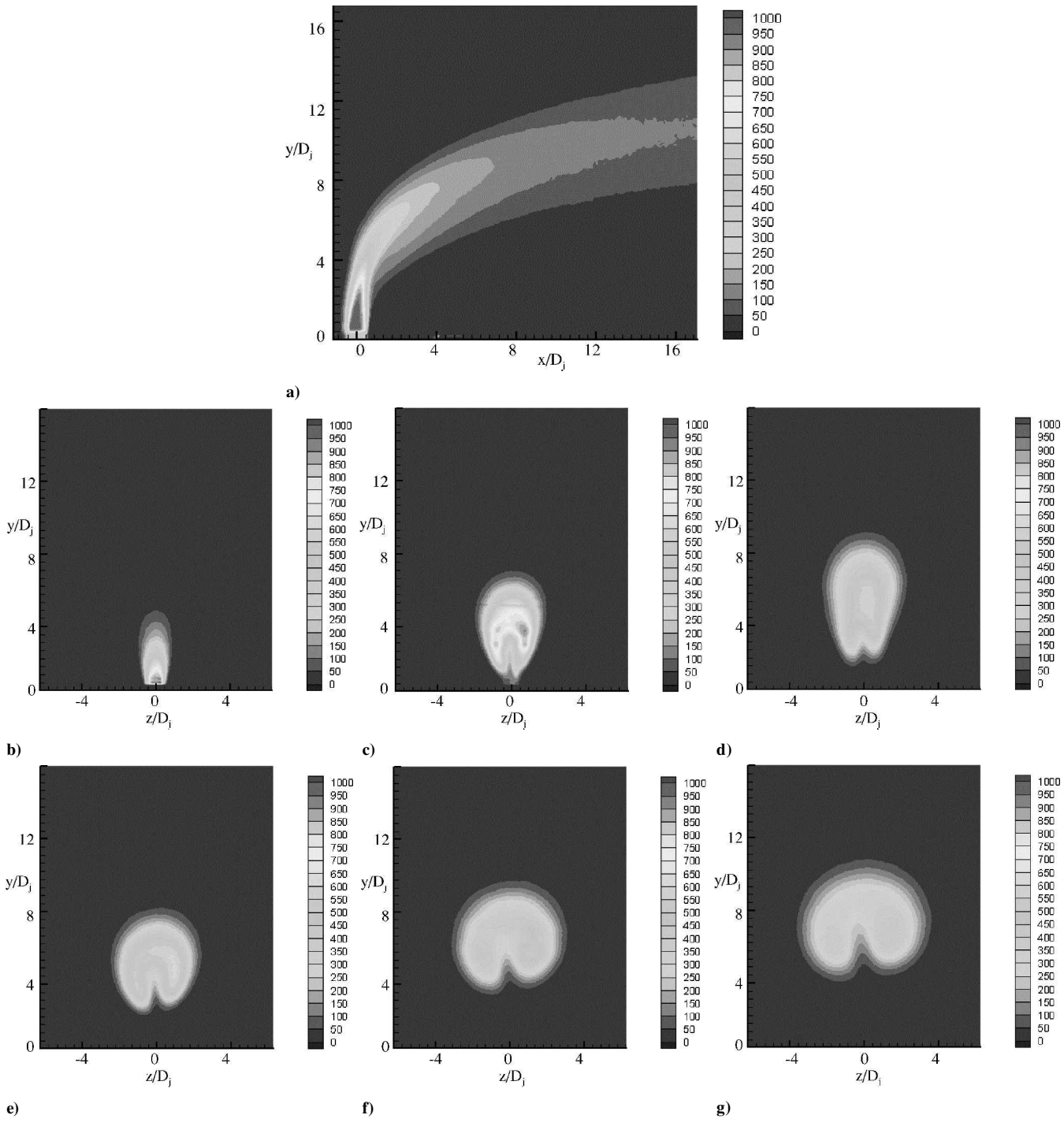

Fig. 4 Time-averaged scalar intensity images of the unforced jet in crossflow, displaying a) streamwise (through the spanwise jet centerline) and crossstream planes at x/D_j = b) 0, c) 1, d) 2, e) 3, f) 4, and g) 6, downstream of the jet exit plane.

denoted is the streamwise extent over which most of the cross-stream measurements presented in the forthcoming sections were recorded. The jet instabilities, originating as the shear layer structures, and the far-field CVP structure are evident. There is little evidence of jet fluid in the wake region. The instantaneous cross-stream plane image (Fig. 3b) clearly shows an asymmetric flow pattern. Such a pattern is far from the idealized and simplified picture of the jet-in-crossflow comprising a pair of symmetric counter-rotating vortices.[10] The cross-stream structure is quite complex and appears to comprise several smaller scale vortices (perhaps originating from the jet shear layer) and will be addressed later. The instantaneous and time-averaged scalar structure of the jet in crossflow was the subject of detailed investigations by Smith and Mungal.[16] Of particular interest was the asymmetry in the time-averaged crossplane flow images.

Figure 4 shows the time-averaged images (streamwise and cross stream) of the scalar (smoke particles), showing the jet bending into the cross stream, and a nearly symmetric pattern arising from the CVP dynamics at downstream locations. Figure 5 shows the time-averaged velocity field in cross-stream planes located downstream of the jet exit plane. Note that the measured mean velocity was dominated by the vertical jet velocity in the jet core region of the first cross-stream plane (Fig. 5a), whereas the axial velocity component dominated in the freestream region. The bending of the jet into the crossflow and its cross-stream entrainment is evident in the spreading velocity distribution. Slight asymmetries were observed

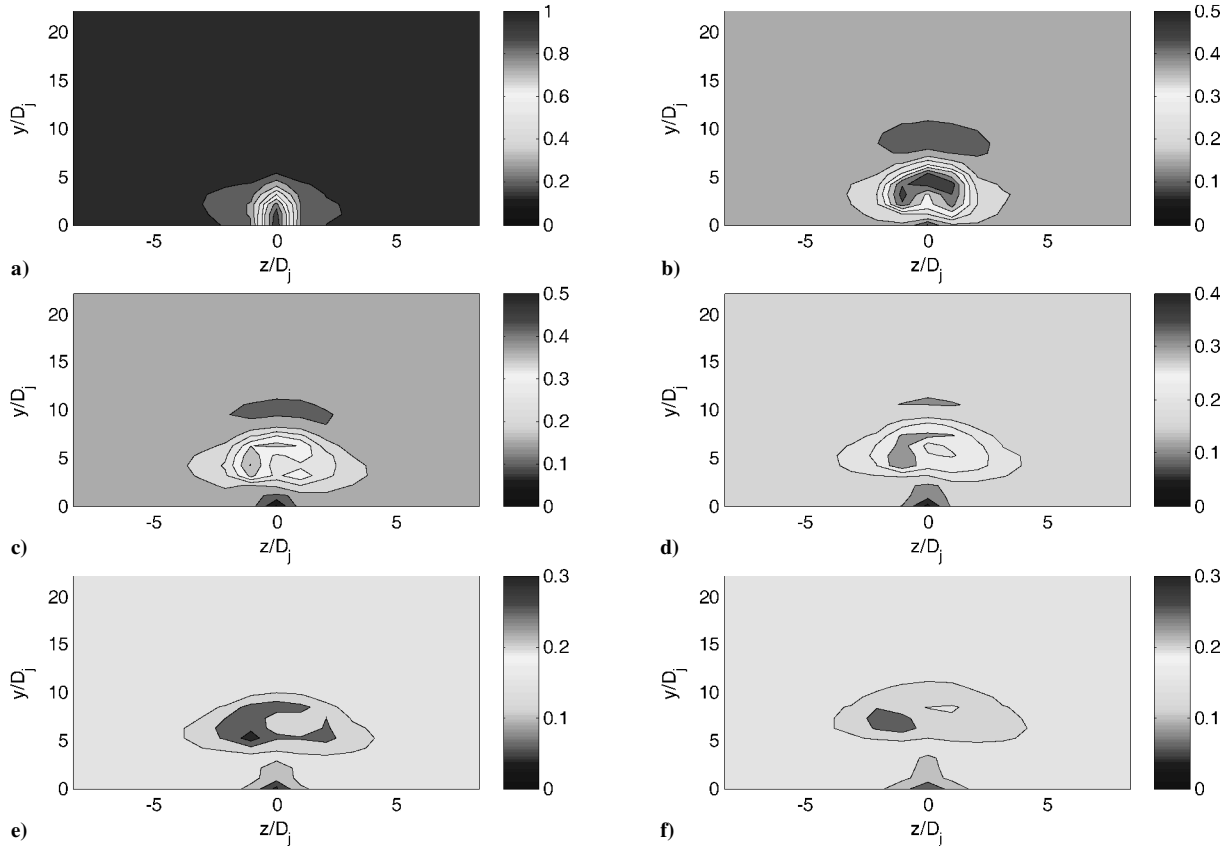

Fig. 5 Time-averaged longitudinal velocity field in unforced flow, with velocity normalized by peak inlet jet velocity, displaying cross-stream planes at x/D_j = a) 0, exit plane for unforced jet in crossflow, b) 1, c) 2, d) 3, e) 4, and f) 6, downstream of jet exit.

in the crossflow pattern in the scalar images (Figs. 4c–4g) and in the velocity fields (Figs. 5b–5f). These may be due to inadequate averaging in downstream locations, where much lower frequency modulations were observed. The asymmetries are similar to those noted farther downstream in phase-averaged scalar images by Smith and Mungal,[16] who explored this in further detail. No asymmetries were found in the jet or the crossflow with the exception of small secondary flow structures at the four corners of the channel.

The corresponding turbulence intensity distributions are shown in Fig. 6. The initially high-turbulence intensities concentrated in the jet core migrated and accumulated in regions where the unsteady (large-scale) mixing of the CVP was dominant. The scales on the contour plots for the mean and fluctuation quantities have been adjusted at various locations to better illustrate the spatial structure; the scales at a given location are, however, maintained for ease of comparison with other cases to be presented later.

The dynamics of the unforced jet were also explored via measurements of the velocity spectra using a single hot-film probe along the jet trajectory. Measurements close to the jet exit did not reveal distinct frequency peaks associated with the shear layer modes, possibly due to the thick boundary layers in the pipe leading up to the jet exit. Similar measurements were reported recently by Shapiro et al.,[17] where power spectra of the velocity measured in the upstream shear layer of the jet revealed broadband spectral peaks corresponding to $0.5 < Sr_D < 0.8$; these are consistent with the initial jet shear layer scales and dynamics. Such broadband peaks are expected to shift to lower frequencies in the range $0.3 < Sr_D < 0.5$ (corresponding to the large scales of the preferred mode of a jet) farther away from the jet exit plane and closer to the end of the jet potential core, for example, see Fig. 5a. This was also found in the studies of Blossey et al.[2]

Velocity surveys were conducted in the flow region where the jet bent into the cross stream. Figure 7 shows velocity spectra with broadband peaks surrounding much lower frequencies than expected in the near field of an isolated jet, such as $Sr_D \approx 0.03$, 0.08, and 0.1. These locations farther from the jet exit (stations 1, 2, and 3 in Fig. 7) were chosen to be close to where the CVP structure was formed. The probe was positioned close to the outer edge of the jet shear layer to help discern the large-scale structure passage frequency. The spectra suggest that low-frequency oscillations were prevalent during CVP formation. When the probe was moved inside the jet at these downstream locations, to reveal further internal details of the CVP structure, the spectra were masked by broadband behavior with no discernible dynamics.

Based on the preceding observations, we attempt to establish a connection between the timescales of the jet flow structures (scaling with D_j) and those associated with the CVP (scaling with $r D_j$). Detailed experimental evidence for the associated spatial structure does not exist, leading to speculations while remaining consistent with the observations. The dynamics near the CVP formation region are associated with lower frequencies than expected from jet vortex dynamics. Therefore, it appears that these dynamics were excited and sustained by the collective behavior of several jet structures. The jet itself evolves via vortex mergers from high-frequency smaller scale structures appearing near the jet origin to lower frequency, larger structures appearing away from the jet exit [(x, y) plane images in Figs. 3 and 8a]. Instantaneous scalar images (Fig. 3) clearly show the quasi regularly spaced flow structures on the upstream edge of the jet, with progressively growing scales along the jet trajectory. Any distinct structure in the aft portion of the jet was lacking. It is plausible that the lower portion of the jet vortices was reoriented, with vorticity aligned in the streamwise direction (as for the CVP). The complex crossflow pattern noted in the instantaneous scalar image in Fig. 3 is also indicative of smaller scale vortices in the cross-stream structure (perhaps originating from the jet vortices).

A simplified conceptual picture for the evolution of the near field of a jet in crossflow is presented schematically in Fig. 9. Only flow structures associated with the jet shear layer and the CVP are treated.

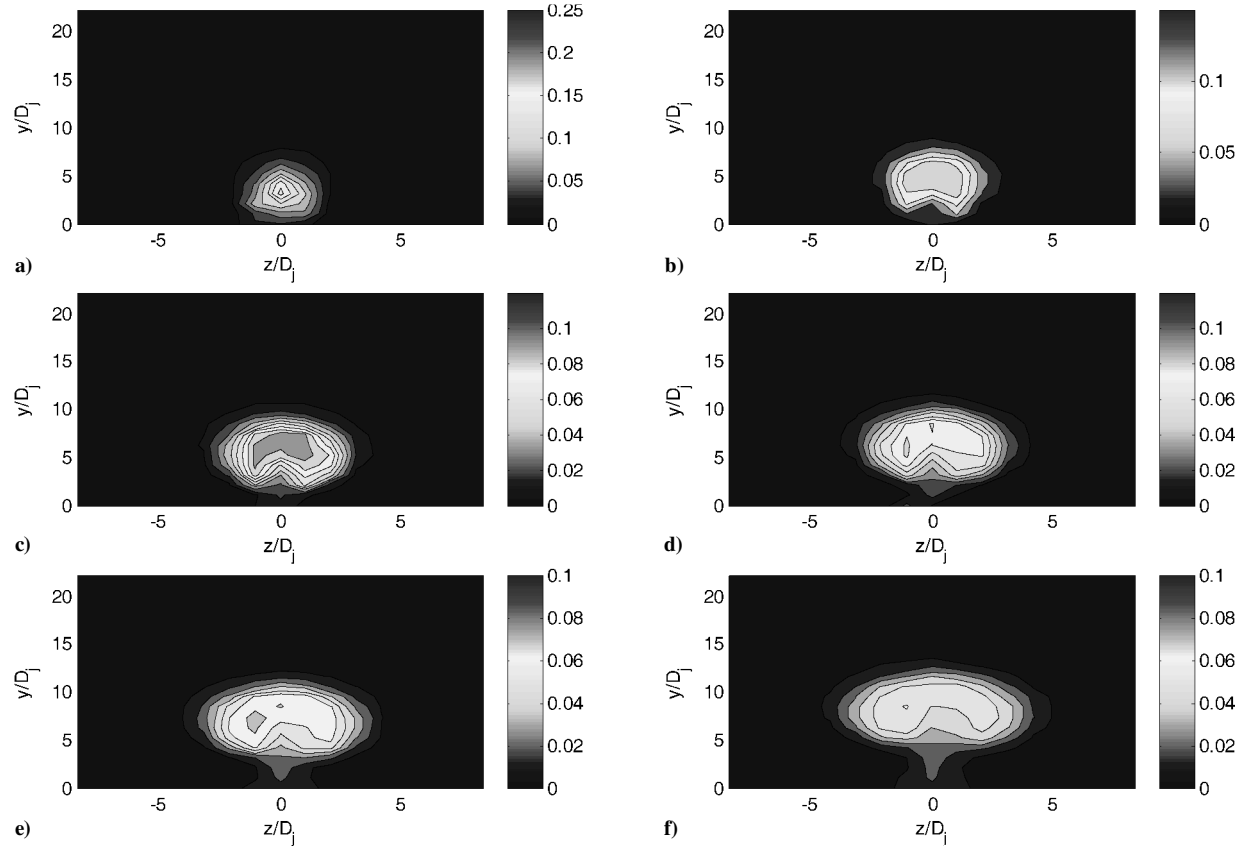

Fig. 6 Time-averaged fluctuating component of longitudinal velocity field in unforced flow normalized by peak inlet jet velocity; cross-stream planes at x/D_j = a) 0, exit plane for jet in crossflow, b) 1, c) 2, d) 3, e) 4, and f) 6, downstream of jet exit.

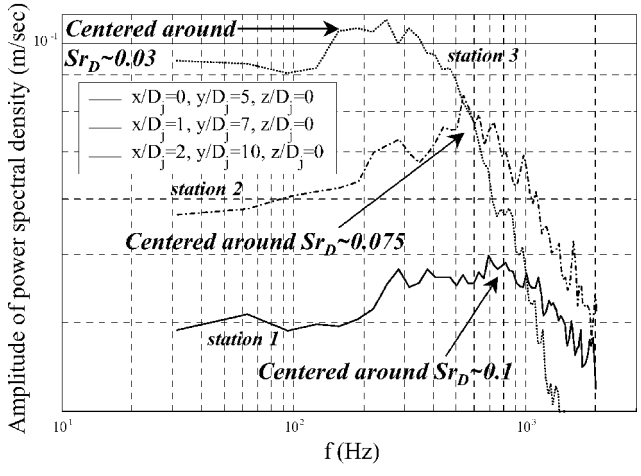

Fig. 7a Velocity spectra from unforced jet in crossflow measured at three locations along the jet trajectory, displaying broadband peaks at progressively lower frequencies as the probe is moved farther from the jet exit.

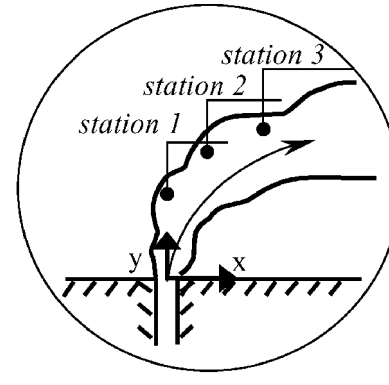

Fig. 7b Probe locations corresponding to measurements shown in Fig. 7a.

The mechanism for the transition of high-frequency oscillations near the jet exit to lower frequency dynamics farther downstream is speculated to be from the growth and merger of the jet vortices on the front side and due to the agglomeration of the lower portion of the jet vortices in the aft side of the jet. Physical mechanisms involving three-dimensional vortex dynamics that support such a connection between the jet shear layer vortices and the CVP have been proposed before,[8–10] although details of the CVP formation are not yet fully resolved. The present data and inferences are consistent with these prior hypotheses. Although no conclusive evidence is presented for the CVP formation, a promising avenue for controlling mixing is revealed. This involves manipulation of the spacing and dynamics of the jet shear layer structures and is explored further in the next section.

B. Forced Response Experiments

Frequency-sweep experiments were conducted to examine the unsteady response of the jet-in-crossflow to single-frequency excitation. No crossflow was applied for these tests, which were performed for fixed control signal input amplitude to the actuator, that is, the pressure at which the air was supplied to the actuator was held constant. Figure 10a shows the nonuniform frequency response of the unsteady actuator flow to forcing (with no crossflow). The fluctuation amplitude decreased with increasing frequency because the tubes and passages outside the valve (leading to the jet exit) behave as capacitors, reducing the velocity amplitude at higher frequencies. The nonuniform response, for instance around 1000–1600 Hz, could

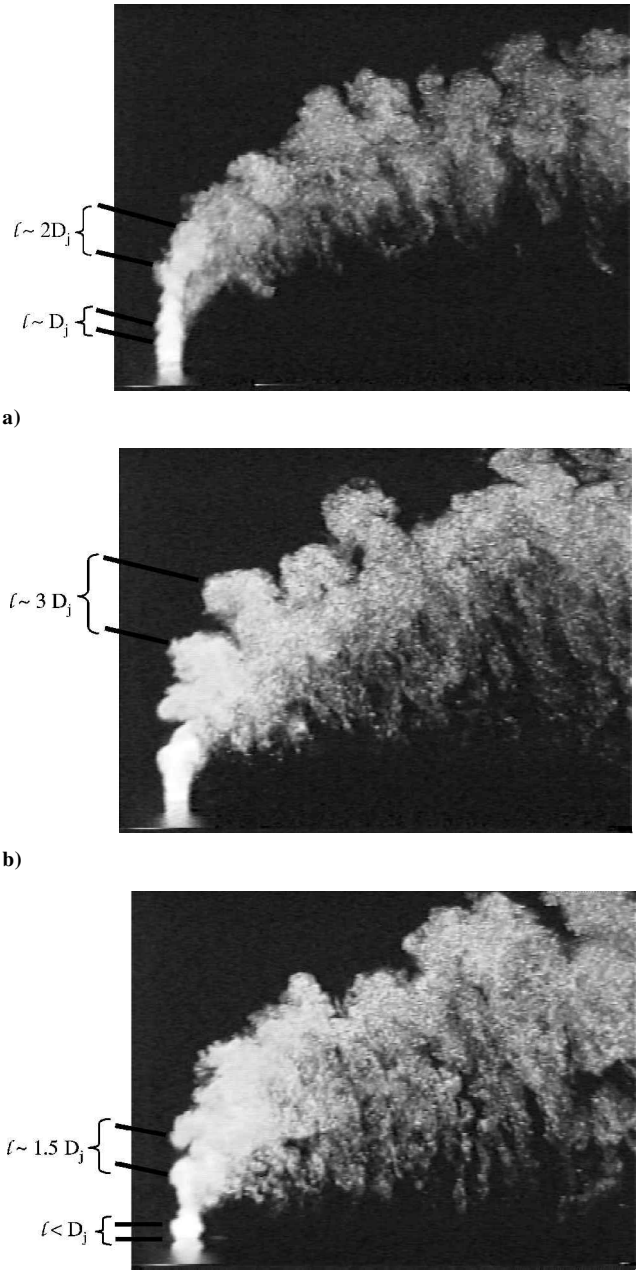

Fig. 8 Instantaneous scalar images of unforced and forced flowfields: a) unforced flow, b) forced flow, showing fewer, larger (evenly spaced) structures for low-frequency forcing $f = 680$ Hz ($Sr_D \sim 0.085$), and c) showing smaller structures closer to the jet injection location for high forcing frequencies, 1500 Hz ($Sr_D \sim 0.19$).

result from the acoustic characteristics of the passages outside the valve leading to the jet exit, which would enhance the signal amplitude at preferred frequencies. Note that unlike traditional zero-mass-flux actuators, for example, acoustic excitation, this actuation scheme has a nonzero mean flow; also recall discussion in Sec. II. Notice the slight variation in the mean flow exiting the actuator (about 7%), which caused a concomitant variation in the velocity ratio established. The nearly monotonic reduction in the mean velocity with increasing frequency appears to have been caused by lower leakage in the valve at higher rotational speeds. This may have been due to better control of leakage areas from centrifugal and thermal expansion at the higher speeds. Such differences were accounted for by changing the supply pressure to maintain the same mean velocity ratio.

Figure 10b shows an example of the (bandpass filtered) velocity signal measured $2D_j$ vertically above jet exit for forcing at 680 Hz,

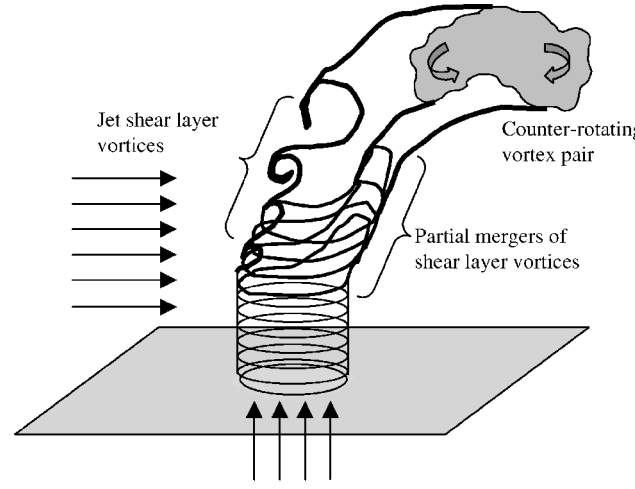

Fig. 9 Schematic of unsteady vortex dynamics underlying the jet in crossflow, indicating dynamics of the jet shear layer vortices and that of the CVP observed after the jet bends into the cross stream.

with a mean velocity of nearly 25 m/s and partial modulation (with a peak-to-peak amplitude of nearly 30% of the mean jet exit velocity). Figure 10c shows a similar example of the (bandpass filtered) velocity signal for forcing at 1500 Hz, with a mean velocity of nearly 24 m/s and modulation with peak-to-peak amplitude of nearly 25% of the mean jet exit velocity. For both cases, crossflow was also employed (with $r = 6$) to evaluate the actual forcing signal appearing inside the jet with crossflow. Such signals were not expected to be as periodic as the waveform that exited the actuator in isolation. The slight modulations were due to low-frequency oscillations present in the crossflow within the test section and the jet disturbances. Because of the nonuniform actuator response, the velocity fluctuation amplitude measured in the forced flowfield was normalized with the fluctuation amplitude measured near the exit of the spinning valve actuator. Because of the nearly sinusoidal nature of the forcing signal observed inside the flow, such normalization appears to suffice. More complex compensation was found to be necessary by M'Closkey et al.[7] when imposing square wave excitation signals with precisely controlled duty cycles.

The velocity fluctuation response to single-frequency forcing over a range of frequencies is shown in Fig. 11. Probe locations were chosen (Fig. 11b) close to the jet exit, in a region where the jet was bending into the crossflow and in a region where the jet was completely bent into the crossflow; the spanwise probe location for the following measurements was chosen to be at the center of the channel where the (x, y) plane intersects the jet exit centerline. The preferential flow response to higher frequencies, namely, $Sr_D \sim 0.2$, in the vertical portion of the jet and to low frequencies, namely, $Sr_D \leq 0.1$, farther downstream is evident; the location in the vertical portion of the jet is situated (vertically) past the end of the jet potential core. (Also see mean velocity shown in Fig. 5a and where the jet turbulence levels reach a peak in Fig. 6a.) Frequency-response measurements indicated that progressively lower frequency dynamics were preferentially excited farther along the jet trajectory. Such receptivity to low-frequency excitation in the downstream flow region (with the CVP structure) and to high-frequency excitation in the initial jet (with shear layer structures) is consistent with the description in the preceding section and shown in Fig. 9. These measurements also revealed the excitable dynamics in the flowfield, which are distributed in space and over a fairly broad range of frequencies. The impact of forcing these receptive bands of frequencies on the flowfield is discussed in the next section.

Figure 12 shows velocity spectra for fixed-frequency forcing, recorded along several locations of the forced flow jet trajectories. Also shown is the broadband low-frequency oscillations centered at 600 Hz (Fig. 12c and circled range, Fig. 12d) for high-frequency forced cases in locations away from the jet exit plane. The probe coordinates are denoted in the Fig. 12 legend and are different for

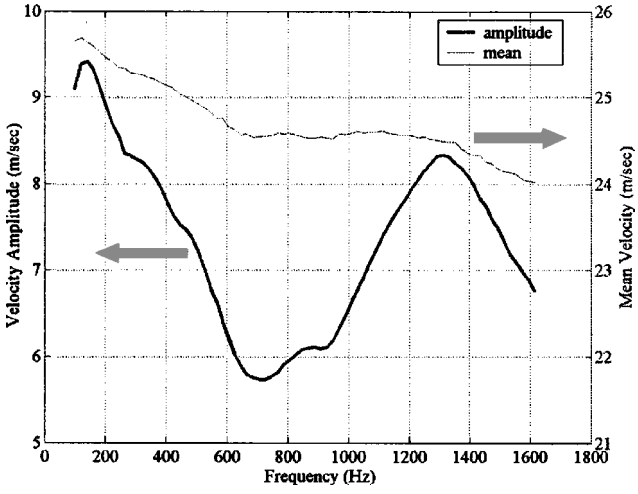

Fig. 10a Spinning valve actuator response to excitation, showing peak amplitude of forcing and mean flow (that is, average jet velocity) as function of forcing frequency.

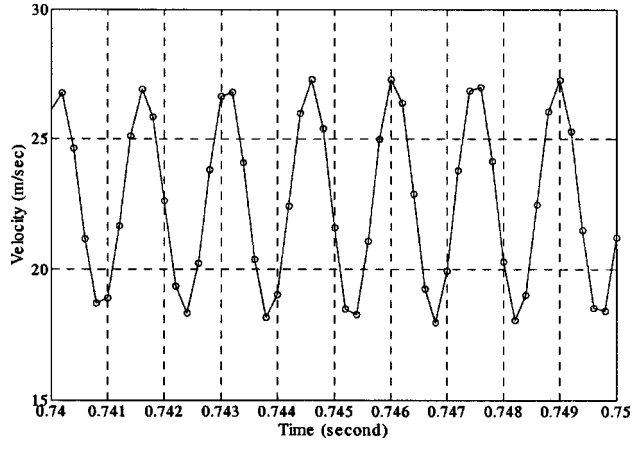

Fig. 10b Velocity signal recorded near the jet exit with actuator operating at 680 Hz.

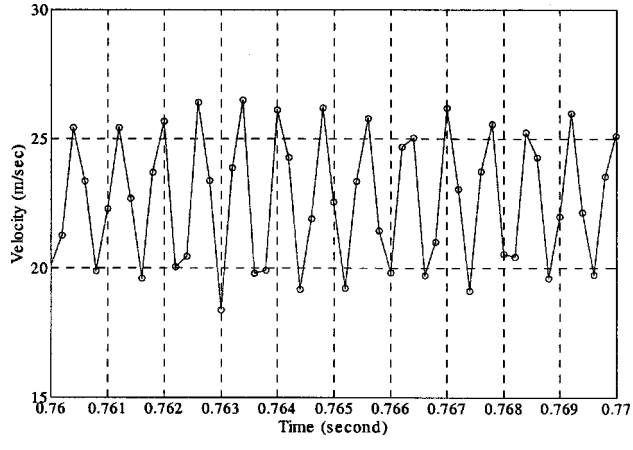

Fig. 10c Velocity signal recorded near the jet exit with actuator operating at 1500 Hz.

the four cases because the locations were chosen to best reflect the local coherent dynamics with minimal contamination from random broadband behavior. Spectral peaks at the excitation frequencies were evident in the velocity spectra closest to the jet exit. Harmonics of the forcing frequency were also evident in all of the spectra recorded close to the jet exit. This suggests that the forcing signal was amplified to high levels, triggering nonlinear interactions between the excitation frequency and its harmonics. It was evident

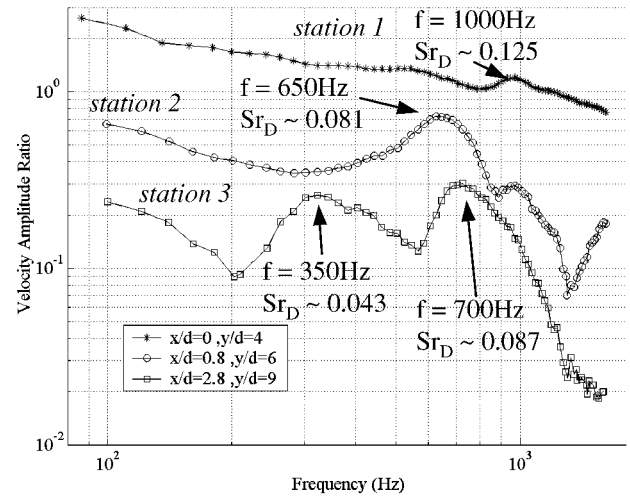

Fig. 11a Frequency response of forced jet in crossflow measured at various locations along jet trajectory ($z = 0$ for all cases).

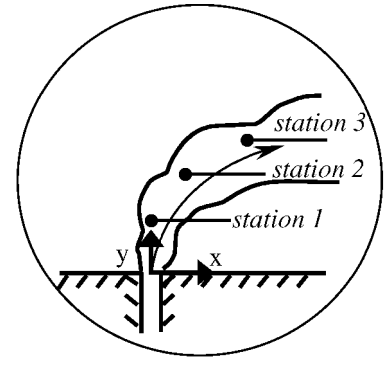

Fig. 11b Three probe locations along the jet trajectory where the frequency response is reported in Fig. 11a.

that the effects of the forcing frequency for $Sr_D > 0.15$ were most pronounced for velocity spectra near the jet exit, whereas the downstream dynamics reverted to a broadband nature. Such broadband behavior was also found in the unforced flow (such as shown at station 1 in Fig. 7). The amplitude at the high forcing frequency also diminished quickly farther downstream. However, forcing at low frequencies ($Sr_D < 0.1$) resulted in amplification and sustenance of the spectral amplitudes farther downstream. This implies organization of the flow structures in a low-frequency band. The result is also consistent with the frequency-response measurements (discussed earlier) at the downstream locations farther from the jet exit, where lower frequencies were considered to be preferentially excited.

C. Open-Loop Control Results

Based on the surveys of the unforced and forced flow responses, it was concluded that, for improved entrainment, penetration, and mixing characteristics of the downstream flow, it would be beneficial to excite the jet flow at low frequencies. The unsteady effects induced would be amplified through instabilities and interactions in the flow and dominate the dynamics farther downstream, where uniform mixing and increased penetration are desired for industrial applications of jets in crossflow.

Figure 8 shows instantaneous snapshots of the unforced and forced flowfields, displaying organization of several smaller flow structures for the flow forced with a high frequency (smaller length scales denoted in Fig. 8c near the jet exit) and fewer larger structures for one forced at a lower frequency. (Length scale is deduced from the flow structure spacing in the outer edge of the jet and is denoted in Fig. 8.) Because of the use of relatively low forcing (or peak-to-peak modulation) levels, the controlled jet flow structures were similar to those in the unforced flow. This contrasts with the

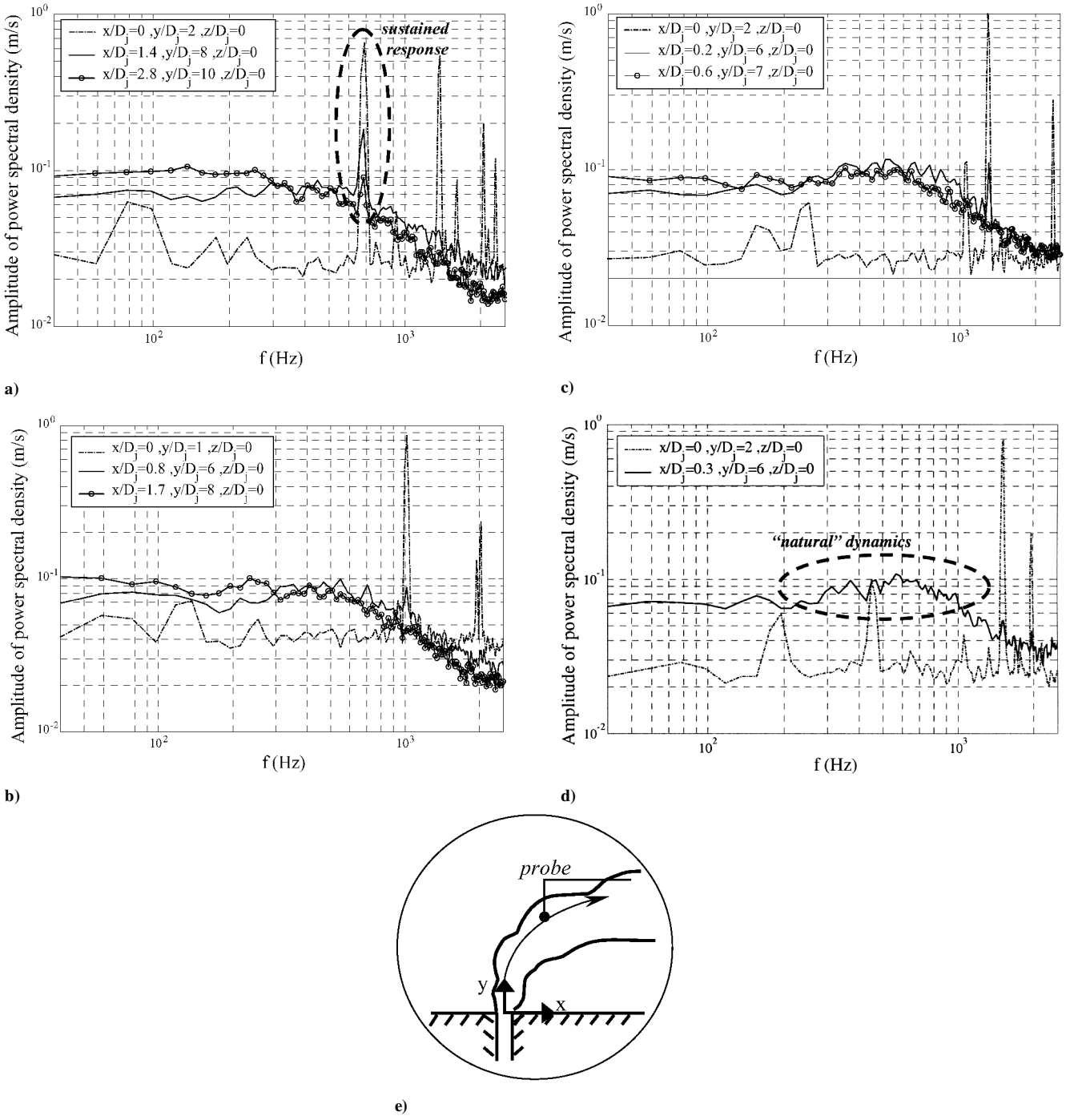

Fig. 12 Velocity spectra of forced jet in crossflow measured at various locations following the jet trajectory showing sustained response to lower forcing frequencies farther from jet exit and damped response to higher forcing frequencies: a) f = 680 Hz ($Sr_D \sim 0.085$) b) f = 1000 Hz ($Sr_D \sim 0.125$), c) f = 1300 Hz ($Sr_D \sim 0.163$), d) f = 1500 Hz ($Sr_D \sim 0.19$), and e) measurement coordinate system for locating the probe along the jet trajectory where the power spectra are recorded.

radically changed jet flow structure, for example, appearance of distinct vortex rings, observed in prior studies utilizing high forcing levels and full jet modulation.[4–6]. There was a noticeable increase in the scalar concentrations in the wake region of the forced jet (Figs. 8b and 8c) relative to the unforced flow (Fig. 8a). Because the nondimensional excitation frequency ($Sr = f D_j / U_\infty$) was in the range $Sr = 0.5$–1 (well outside the natural wake shedding frequency of $Sr = 0.1$–0.2), the mechanism for the enhanced wake unsteadiness is unclear.

Unsteady forcing produced a marginal increase in jet penetration in all forced cases possibly due to the increased time-averaged spread created by flapping of the jet. Figure 13 shows the time-averaged scalar images for the forced case using a forcing frequency of 680 Hz ($Sr_D \sim 0.085$). Cross-stream mixing enhancement relative to the unforced case (see Fig. 4) is evident for $4 \leq x/D_j \leq 6$. Note that the counter-rotating vortex structure evident in the time-averaged scalar images for the unforced jet in cross flow (Figs. 4e–4g) was absent in the forced case, suggesting the modification of this structure as a result of forcing. Further insight into the spatial structure associated with the forced flow can only be obtained via phase-averaged measurements in the flow. Increase in the near-field jet spread in the (x, y) plane (Fig. 13a) relative to that in the unforced jet (Fig. 4a) was also evident, and at least in part may be related to the wake structures seen earlier (Fig. 8b). Cross-stream mixing was

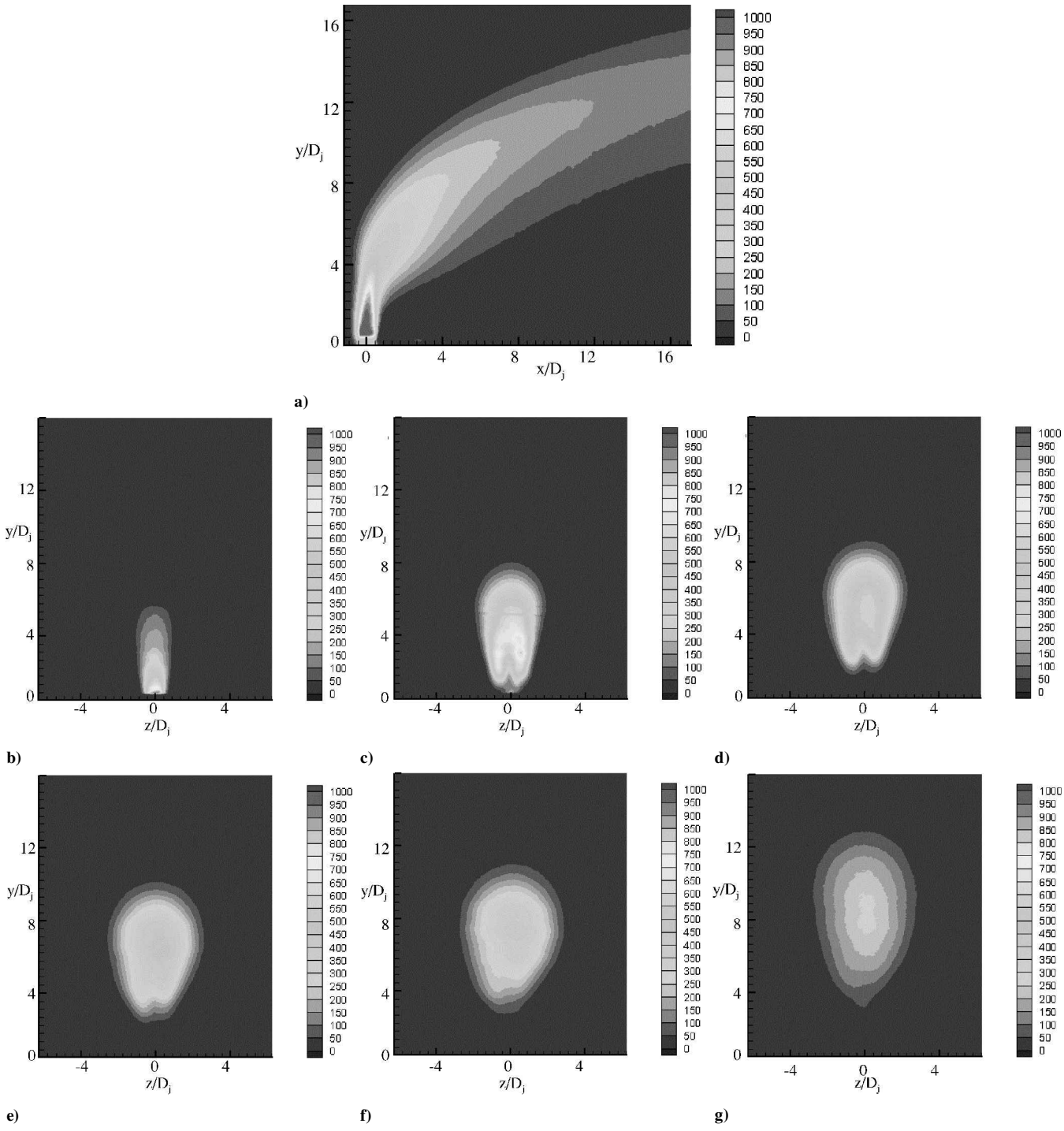

Fig. 13 Time-averaged scalar intensity images of the forced jet ($Sr_D \sim 0.085$) in crossflow: a) streamwise plane (through the spanwise jet centerline) and cross-stream planes at x/D_j = b) 0, c) 1, d) 2, e) 3, f) 4, and g) 6.

evenly achieved for lower frequency forcing (Fig. 13b–13g) revealing improved and uniform spreading in both the transverse and spanwise directions. The uniform cross-stream mixing (showing lower peak scalar levels) farther downstream is evident.

Conversely, more compact spanwise mixing and increased transverse/vertical mixing was observed for the high-frequency forced case as shown in Fig. 14 (where $f = 1500$ Hz and $Sr_D \cong 0.19$). Here, mixing was significantly enhanced close to the jet exit (Fig. 14a–14d compared with Fig. 4a–4d) for the unforced flow), but peak scalar levels remained higher farther downstream (due to reduced uniformity in mixing). The increased mixing in the vertical direction is evident, as is the relatively lower spanwise mixing. In particular, it is evident from Fig. 14e–14g, for $4 \leq x/D_j \leq 6$, that the extent of scalar spread in the transverse direction was more than that in the spanwise direction, where the spread was compact in that it was even smaller than in the unforced flow. Increase in the near-field jet spread in the (x, y) plane (Fig. 14a) relative to that in the unforced jet (Fig. 4a) is more dramatic here (compared to that in Fig. 13a) due to potentially direct excitation of the jet vortices. Although spread increase in this plane due to excitation of wake structures discussed earlier (Fig. 8c) is possible, this coupling of the forcing into the wake unsteadiness is not expected to be any more effective than for the low-frequency case considered earlier.

Figures 15 and 16 show the time-averaged velocity in cross-stream planes downstream of the jet exit plane for the lower (680 Hz) and higher (1500 Hz) forcing frequency cases, respectively. As for the unforced flow, the velocity fields shown must be interpreted carefully, noting that measurements on the crossplane intersecting

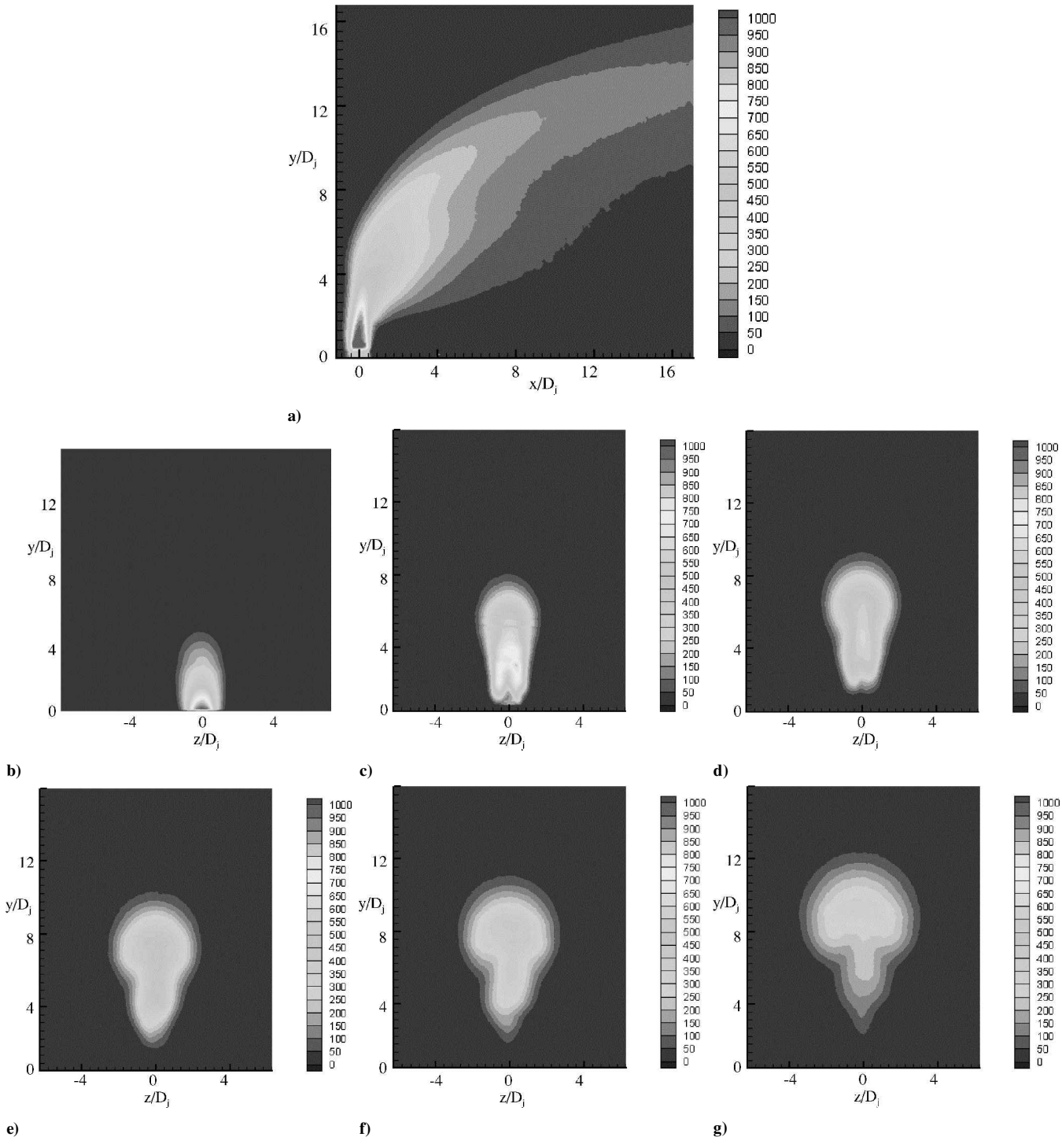

Fig. 14 Time-averaged scalar intensity images of the forced jet ($Sr_D \approx 0.19$) in crossflow: a) streamwise plane (through the spanwise jet centerline) and cross-stream planes at x/D_j = b) 0, c) 1, d) 2, e) 3, f) 4, and g) 6, downstream of the jet exit plane.

the incoming jet axis (Figs. 15a and 16a) show the vertical velocity component inside the jet core and the axial velocity component in the freestream. For downstream crossplanes, the axial velocity component was measured uniformly across the entire plane. Note that the contour plot scales at any location are consistent with that for the unforced flows (shown earlier). The improved entrainment for the low-frequency forcing case can be qualitatively seen in downstream crossplanes (compare with contour levels for unforced flow in Fig. 5), with lower levels of the axial velocity component spread out farther in the spanwise and vertical directions.

For quantitative comparisons, the entrainment ratio was computed from the mean velocity distributions in the unforced and forced flows. The entrainment ratio is defined as the ratio of the volumetric flux across a downstream crossplane (for the out-of-plane axial velocity component) to that across the horizontal inlet plane of the jet, namely, for the vertical velocity at the lower horizontal wall. Only contributions to the flow from the jet were included. The volumetric flux at x_0 is defined as

$$\equiv \int_A U(x_0, y, z)\, \mathrm{d}y\, \mathrm{d}z$$

where U denotes the local axial mean velocity and the integration was performed over the area A where the jet fluid is distributed. The jet fluid area A is determined by computing the area inside the boundaries over which the time-averaged scalar values drop to 1% of

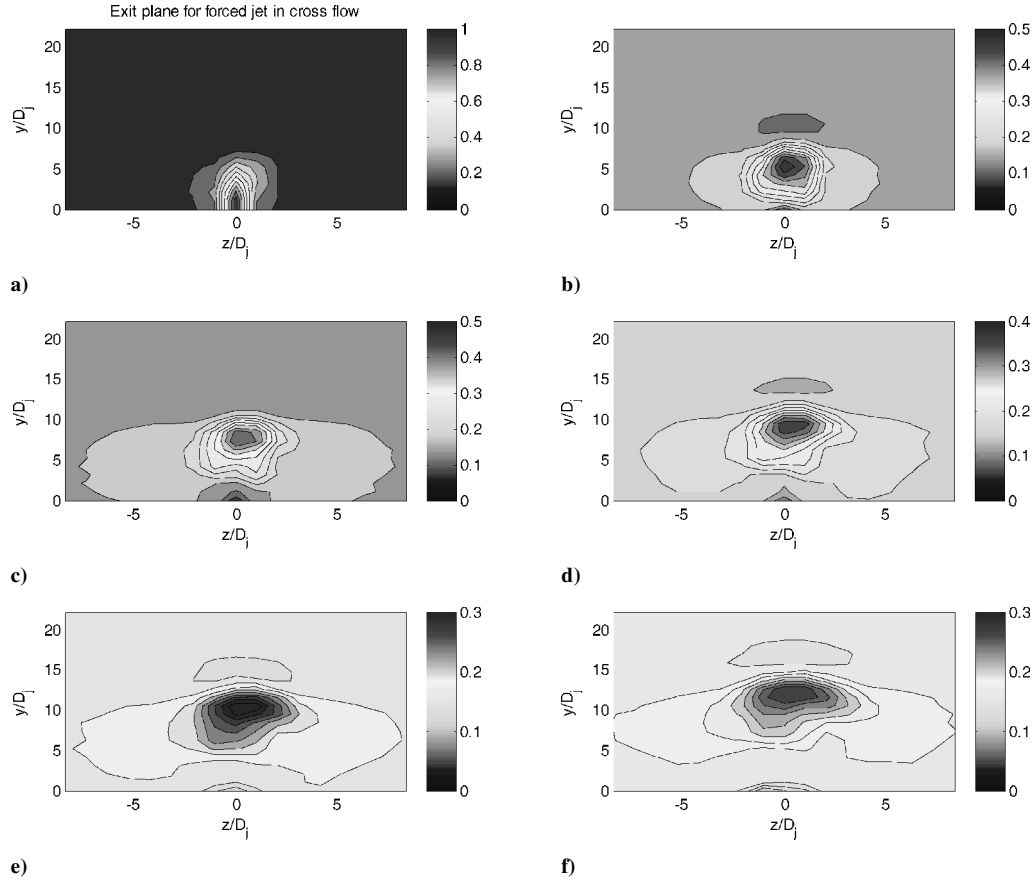

Fig. 15 Time-averaged longitudinal velocity field in forced flow ($Sr_D \sim 0.085$) with velocity normalized by peak inlet jet velocity; cross-stream planes at x/D_j = a) 0, b) 1, c) 2, d) 3, e) 4, and f) 6.

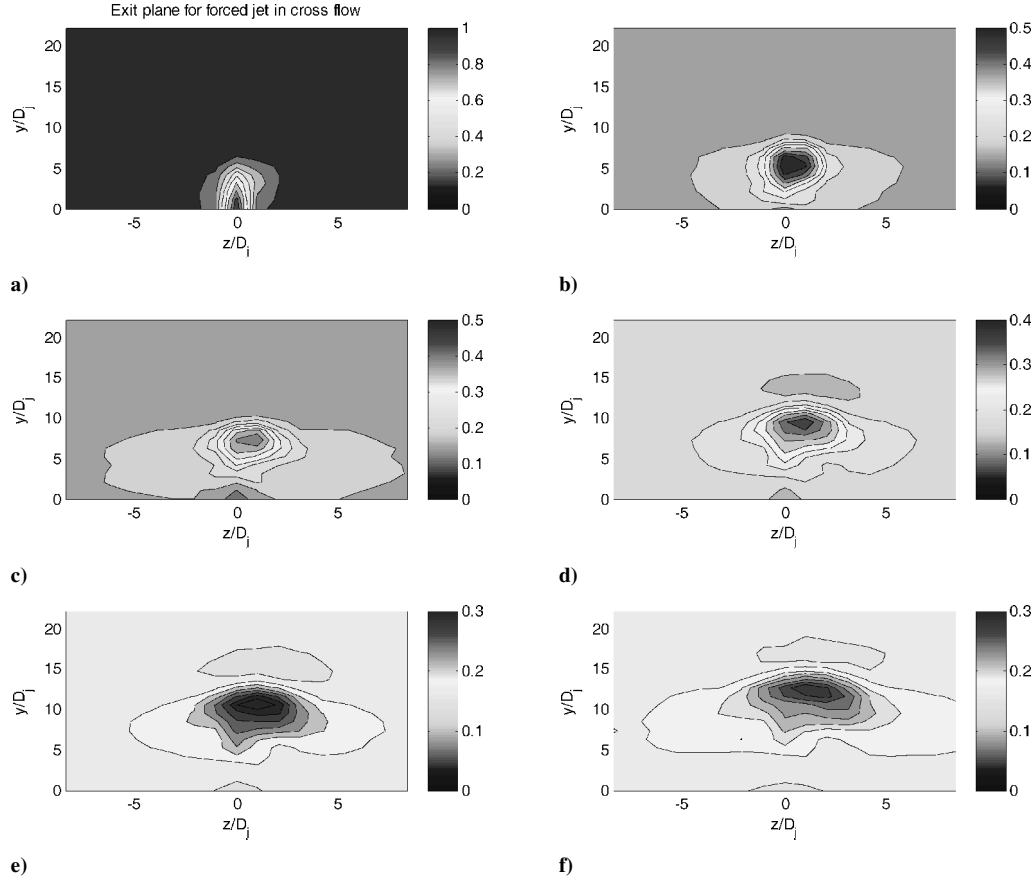

Fig. 16 Time-averaged longitudinal velocity field in forced flow ($Sr_D \sim 0.19$) with velocity normalized by peak inlet jet velocity; cross-stream planes at x/D_j = a) 0, b) 1, c) 2, d) 3, e) 4, and f) 6.

the local peak values in the jet (Figs. 4, 13, and 14); note that because only the jet was seeded with smoke in the scalar measurements, such a threshold set on jet scalar values is justified. This entrainment parameter definition was used by Yuan and Street,[18] who studied the sensitivity of entrainment computations to the scalar threshold and determined the 1% value to be acceptable in simulations of a round jet in crossflow. To ensure that the mean jet trajectory differed only slightly from the crossflow direction, crossplanes only downstream of where the jet bent into the cross stream were examined, namely, $x/D_j \geq 1$. Figure 17 shows the entrainment ratio computed at five streamwise locations downstream of the jet exit using mean velocity data. The evident entrainment ratio increase with downstream distance for the unforced flow is consistent with prior experiments and simulations, with a power-law dependence on the streamwise coordinate. Enhancements of 30–46% in time-averaged entrainment (relative to that for the unforced jet) at planes from $1 \leq x/D_j \leq 5$ (measured from the incoming jet axis) were seen for the forced flows, namely, $Sr_D \cong 0.09$ and 0.19. These measurements demonstrate the benefit of unsteady forcing. The enhancements are similar for the two forced cases, with slightly improved benefits for the lowest forcing frequency case, namely, $Sr_D \cong 0.09$. Nevertheless, the entrainment ratios for the forced flows are consistently higher than that for the unforced flow.

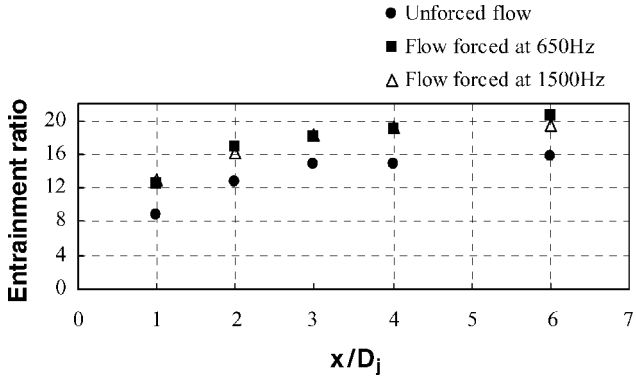

Fig. 17 Entrainment ratio variation with downstream distance from (vertical) jet axis in unforced and forced flows; sustained improvements for forced cases are evident.

Figures 18 and 19 show the turbulence intensity fields in the forced flows, where $f = 680$ Hz and $Sr_D \sim 0.085$ and $f = 1500$ Hz and $Sr_D \sim 0.085$, respectively. Here, too, the contour plot scales at any location are set to be consistent with that for the unforced flows (shown in Fig. 6). In Figs. 18 and 19, fluctuation is normalized by peak inlet jet velocity. In general Figs. 18 and 19 reveal increased (temporal) unsteadiness in the jet mixing over a larger crossplane region (compared to the unforced jet), which accompanies the jet entrainment increase for the two forced flow cases. Such behavior is desirable for combustion applications, for example, using dilution jets in a fuel-rich crossflow, where spatiotemporally uniform mixing is desired. Differences between the turbulence intensity fields for the two forced flow cases were difficult to discern. However, shapes of the downstream flowfields (Figs. 18d–18f and 19d–19f) showed differences similar to those observed in the mean velocity fields. Assessments of the entrainment and mixing enhancements across

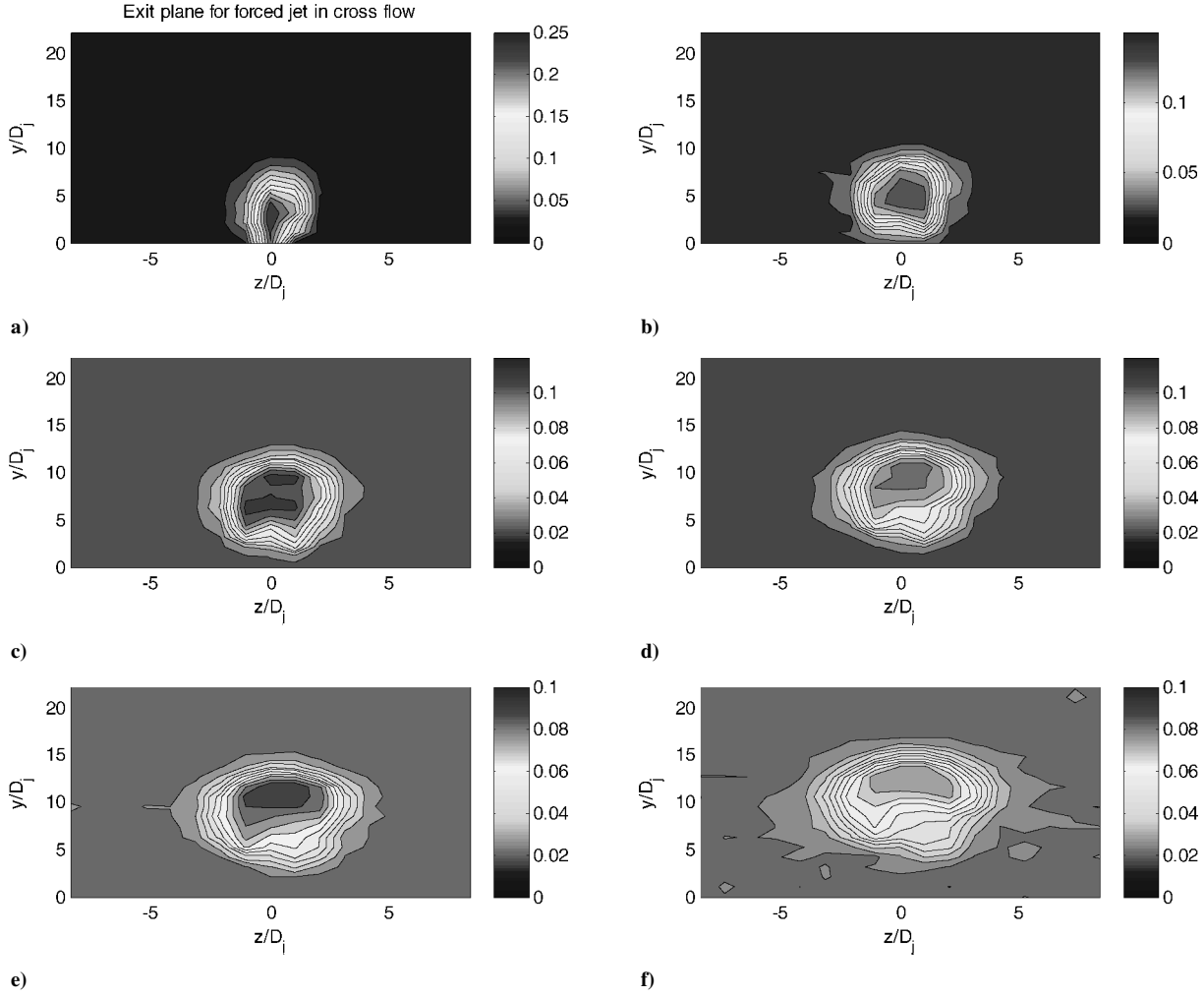

Fig. 18 Time-averaged fluctuating component of longitudinal velocity field in forced flow ($Sr_D \approx 0.085$); cross-stream planes at x/D_j = a) 0, b) 1, c) 2, d) 3, e) 4, and f) 6.

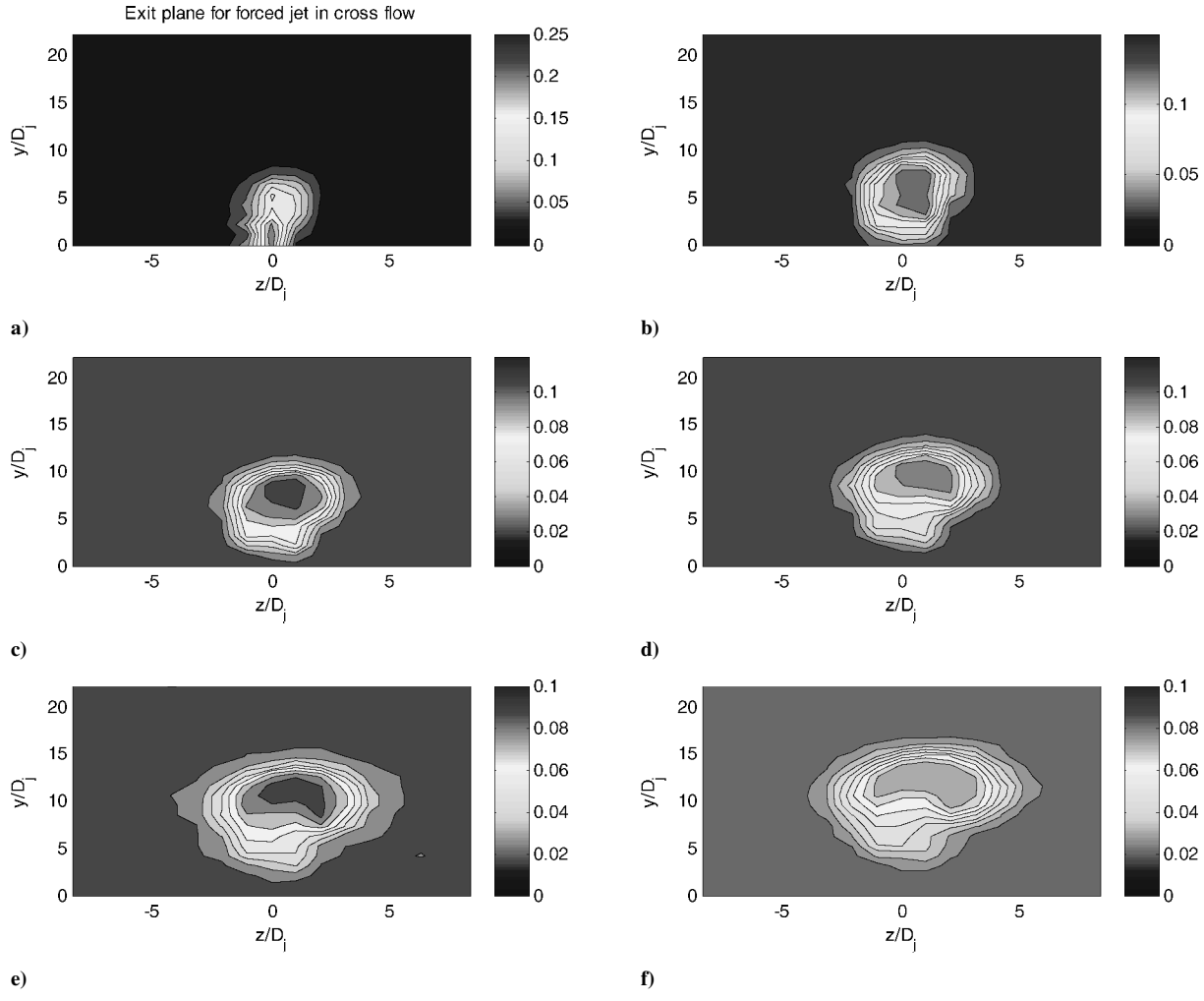

Fig. 19 Time-averaged fluctuating component of longitudinal velocity field in forced flow ($Sr_D \approx 0.19$); displaying cross-stream planes at x/D_j = a) 0, b) 1, c) 2, d) 3, e) 4, and f) 6.

a wider range of forcing frequencies are needed to confirm these trends.

IV. Conclusions

An experimental study of the dynamics of large-scale, organized structures in the near field of a jet in crossflow was performed. The coupling between the dynamics of the jet shear layer and that associated with the formation of the CVP was explored and utilized for open-loop control. It was demonstrated that the structure and mixing of the flow are substantially altered by unsteady forcing.

Experiments were performed in a moderate Reynolds number, isolated circular jet issuing into a uniform cross flow in a square channel, with a velocity or blowing ratio of 6. Receptivity of the flow to high frequencies near the jet exit (commensurate with excitation of jet instabilities) and to low frequencies farther downstream (where the CVP was evident) was established. This was done using forced response experiments in which velocity cross spectra (relative to the forcing signal) were measured in different flow regions to reveal preferential flow response within certain frequency bands. Low-frequency forcing was observed to be the most effective means to organizing unsteadiness in the flowfield downstream of the jet exit plane, where enhanced entrainment and mixing are desired. The scales of the jet vortices increased as the jet emanated and bent into the crossflow, organizing the dynamics into lower frequency bands along the jet trajectory. Furthermore, these low-frequency oscillations were coherent and were sustained at downstream locations where the CVP motion was prevalent.

Measurements of the time-averaged velocity as well as scalar fields revealed increased mass entrainment and coherent unsteadiness as a result of unsteady forcing. The jet spread and mixing benefits were demonstrated for a pair of forcing frequencies chosen at the lower and higher end of the actuator frequency response. Jet spread was enhanced near the jet exit for the high forcing frequency case, consistent with the findings from the forced response tests. At locations downstream of the jet exit, where lower frequencies are preferentially amplified, the spatial uniformity of mixing when forced at a lower frequency was found to be better than that for the flow forced with a higher frequency.

More detailed exploration of the control parameter space is necessary, including studies of the effects of forcing amplitude, waveform, and a larger range of forcing frequencies; the latter was limited in this study due to the actuator bandwidth. Further studies of the effects of forcing on a variety of mixing metrics, in addition to mass entrainment and jet spread, such as for the (spatial) uniformity of mixing are also needed. Some explorations along these lines were reported by Blossey et al.[2] using direct numerical simulations.

Acknowledgments

This work was supported in part by internal funding from the United Technologies Research Center and in part by the Air Force Office of Scientific Research through Contract F49620-01-C-0021. The authors thank Dave Liscinsky and Andrzej Banaszuk for insightful discussions and suggestions and Bruce True for valuable assistance in the experiments.

References

[1] Bender, E. E., Miller, D. N., Vermuelen, P. J., and Walker, S. H., "Simulation of Pulsed Injection in a Cross Flow Using 3-D Unsteady CFD," AIAA Paper 2000-2318, June 2000.

[2]Blossey, P., Narayanan, S., and Bewley, T. R., "Dynamics and Control of a Jet in a Cross-Flow: Direct Numerical Simulations and Experiments," *Proceedings of IUTAM Symposium on Turbulent Mixing and Combustion*, edited by A. Pollard and S. Candel, Kluwer Academic, Dordrecht, 2001, pp. 45–56.

[3]Crow, S. C., and Champagne, F. H., "Orderly Structure in Jet Turbulence," *Journal of Fluid Mechanics*, Vol. 48, 1971, pp. 547–591.

[4]Vermuelen, P. J., Chin, C. F., and Yu, W. K., "Mixing of an Acoustically Pulsed Air Jet with a Confined Cross Flow," *Journal of Propulsion and Power*, Vol. 6, No. 6, 1990, pp. 777–783.

[5]Johari, H., Pacheco-Tougas, M., and Hermanson, J. C., "Penetration and Mixing of Fully Modulated Turbulent Jets in Crossflow," *AIAA Journal*, Vol. 37, No. 7, 1999, pp. 842–850.

[6]Eroglu, A., and Breidenthal, R. E., "Structure, Penetration and Mixing of Pulsed Jets in Crossflow," *AIAA Journal*, Vol. 39, No. 3, 2001, pp. 417–423.

[7]M'Closkey, R. T., King, J. M., Cortelezzi, L., and Karagozian, A. R., "The Actively Controlled Jet in Crossflow," *Journal of Fluid Mechanics*, Vol. 452, 2002, pp. 325–335.

[8]Kelso, R. M., Lim, T. T., and Perry, A. E., "An Experimental Study of Round Jets in a Cross-Flow" *Journal of Fluid Mechanics*, Vol. 306, 1996, pp. 111–144.

[9]Cortelezzi, L., and Karagozian, A. R., "On the Formation of the Counter-Rotating Vortex Pair in Transverse Jets," *Journal of Fluid Mechanics*, Vol. 446, 2001, pp. 347–373.

[10]Hasselbrink, E. F., Jr., and Mungal, M. G., "Transverse Jets and Jet Flames. Part 1. Scaling Laws for Strong Transverse Jets," *Journal of Fluid Mechanics*, Vol. 443, 2001, pp. 1–25.

[11]Fric, T. F., and Roshko, A., "Vortical Structure in the Wake of a Transverse Jet," *Journal of Fluid Mechanics*, Vol. 279, 1994, pp. 1–47.

[12]Moussa, Z. M., Trischka, J. W., and Eskinazi, S., "The Near Field in the Mixing of a Round Jet with a Cross-Stream," *Journal of Fluid Mechanics*, Vol. 80, 1977, pp. 49–80.

[13]Pratte, B. D., and Baines, W. D., "Profiles of the Round Turbulent Jet in a Cross Flow," *Journal of Hydronautics*, Vol. 92, 1967, pp. 53–64.

[14]Vranos, A., and Liscinsky, D. S., "Planar Imaging of Jet Mixing in Crossflow," *AIAA Journal*, Vol. 26, No. 11, 1988, pp. 1297, 1298.

[15]Barooah, P., Anderson, T. J., and Cohen, J. M., "Active Combustion Instability Control with Spinning Valve Actuator," American Society of Mechanical Engineers, ASME Paper GT-2002-30042, June 2002.

[16]Smith, S. H., and Mungal, M. G., "Mixing, Structure and Scaling of the Jet in Crossflow," *Journal of Fluid Mechanics*, Vol. 356, 1998, pp. 83–122.

[17]Shapiro, S., King, J., Karagozian, A., and M'Closkey, R. M., "Optimization of Controlled Jets in Crossflow," AIAA Paper 2003-0634, Jan. 2003.

[18]Yuan, L. L., and Street, R. L., "Trajectory and Entrainment of a Round Jet in Crossflow," *Physics of Fluids*, Vol. 10, No. 9, 1998, pp. 2323–2335.

A. R. Karagozian
Associate Editor